Rendiconti
Accademia Nazionale delle Scienze detta dei XL
Memorie e Rendiconti di Chimica, Fisica, Matematica e Scienze Naturali
138° (2020), Vol. I, fasc. 1, pp. 97-102
ISSN 0392-4130 • ISBN 978-88-98075-38-6

Nonadiabatic Quantum Dynamics of OH Electronic Quenchings in Collisions with H^+, H, and Kr

PABLO GAMALLO[1] – ALEXANDRE F. ZANCHET[2]
F. JAVIER AOIZ[2] – CARLO PETRONGOLO[3,*]

[1] Departament de Ciència de Materials i Química Física, Universitat de Barcelona, Spain.
[2] Departamento de Química Física, Facultad de Química, Universidad Complutense, Madrid, Spain.
[3] Istituto per i Processi Chimico Fisici, Consiglio Nazionale delle Ricerche, Pisa, Italy.
* Corresponding author: carlopetrongolo41@gmai.com

Abstract – The OH radical is one of the most abundant molecules of the Universe and plays a prominent role in astrochemistry, where many OH reactions can be affected by nonadiabatic interactions between electronic states. In these processes, quantum-mechanical theories and calculations usefully complement experimental observations yielding radiative and non-radiative observables. To this end, we briefly review the quantum dynamics of three OH and OH* electronic-quenching collisions: $OH(X^2\Pi)+H^+$, $OH(A^2\Sigma^+)+H(^2S)$, and $OH(A^2\Sigma^+)+Kr(^1S)$, without and with proton exchange in the first two reactions. Using *ab initio* MRCI potential surfaces and nonadiabatic couplings, and a rigorous time-dependent wavepacket formalism, we analyze the strength of the couplings, the time mechanisms of the collisions, reaction probabilities, cross sections, and rate constants, giving an overall picture of the initial-state-resolved collision dynamics.

Keywords: excited OH radical; collisional quenching; nonadiabatic dynamics

Riassunto – Il radicale OH è una delle molecole più abbondanti dell'Universo e svolge un ruolo di primo piano nell'astrochimica, dove molte reazioni con OH possono essere influenzate da interazioni non adiabatiche tra stati elettronici. In questi processi, le teorie quantomeccaniche e i calcoli completano in maniera utile le osservazioni sperimentali che producono osservabili radiative e non radiative. A tal fine, esaminiamo brevemente la dinamica quantistica di tre collisioni con "quenching" elettronico di OH e OH*: $OH\ (X^2\Pi)+H^+$, $OH\ (A^2\Sigma^+)+H(^2S)$, e $OH(A^2\Sigma^+)+Kr(^1S)$, senza e con scambio protonico nelle prime due reazioni. Utilizzando superfici di potenziale *ab initio* MRCI e accoppiamenti nonadiabatici, e un rigoroso formalismo a pacchetti d'onda dipendente dal tempo, analizziamo la forza degli accoppiamenti, i meccanismi temporali delle collisioni, le probabilità di reazione, le sezioni d'urto e le costanti di velocità, fornendo un quadro generale delle dinamiche di collisione risolte dallo stato iniziale.

Parole chiave: radicale OH eccitato; smorzamento collisionale; dinamica non adiabatica

1. *Introduction*

In 2019 Güsten *et al.* [1] finally observed HeH^+, first molecule of the early Universe, in a planetary nebula using the quantum-mechanical (QM) rate constant of $HeH^+ + H \rightarrow H_2^+ + He$. These authors thus pointed out again the need for accurate QM dynamical theories and calculations in complementing astrochemical findings. Owing to large energies of many regions of the interstellar medium (ISM), atoms and molecules are in excited or ionized electronic states, coupled by large nonadiabatic effects as we found [2] in $He^+ + H_2 \rightarrow He + H + H^+$, where the nonadiabatic room-temperature rate-constant is ~3 orders of magnitude smaller than the adiabatic one, or in the photodissociation $H_2O + h\nu \rightarrow OH(X^2\Pi + A^2\Sigma^+) + H$, or in the electronic quenching $OH(A^2\Sigma^+) + Q \rightarrow OH(X^2\Pi) + Q$. OH is the fourth most abundant molecule of the Universe, being present in Sun-like stars, red giants, protostars, planets, satellites, comets, and ISM.

The OH electronic quenching by ions and atoms thus plays an important role in astrochemistry, and we here summarize a few nonadiabatic QM results for the gas-phase collisions $OH(X^2\Pi) + H^+$ [3] and $OH(A^2\Sigma^+) + H$ [4], adapting all figures from previous works, and reporting some preliminary findings for $OH(A^2\Sigma^+) + Kr$ [5].

The collisions $OH + H^+$ and $OH^* + H$ open many reactive channels but we here consider only the pure quenching and the proton exchange-quenching that are both observable only in isotopic reactions. These elementary processes are closed in the Born-Oppenheimer approximation and we investigate their QM dynamics via a time-dependent wavepacket method. To this end, we define a total Hamiltonian that contains many rovibronic couplings, using adiabatic or diabatic electronic representations, and we then solve the equation of motion and Fourier transform from time to energy for computing initial-state-resolved reaction probabilities, total integral cross sections, and rate constants.

2. *Theory*

We investigate the dynamics of all reactions using accurate *ab initio* multi-reference configuration-interaction potential energy surfaces (PESs) and couplings: for $OH + H^+$ and $OH^* + H$ see [3, 4] and the preliminary $OH^* + Kr$ calculations extend those of [6]. $OH + H^+$ and $OH^* + Q$ reactions are barrierless and exothermic by about 0.9 and 4.1 eV, respectively.

Following [7], the collision OH+Q is described by reactant Jacobi coordinates R, r, and γ, by a body-fixed reference frame with OHQ in the z,x plane and z along $\boldsymbol{R}$ (R-embedding) or along $\boldsymbol{r}$ (r-embedding), and by a spinless rovibronic Hamiltonian $\hat{H}$ that contains the electronic Hamiltonian $\hat{H}^{\rm el}$ and the total $\hat{\boldsymbol{J}}$ and electronic $\hat{\boldsymbol{L}}$ angular momenta. Nonadiabatic electronic effects are due to $\hat{H}^{\rm el}$ and $\hat{\boldsymbol{L}}$: the former couples two diabatic electronic states [avoided crossing or conical intersection (CI) effects]; the matrix elements of the latter and of the products of its components couple two adiabatic or diabatic electronic states or add up to the PESs [Renner-Teller (RT) effects]. $\hat{H}$ is represented in an orthonormal basis of OHQ electronic, radial grid, associated Legendre $|jK\rangle$, and symmetry Wigner $|K\sigma p\rangle$ states, where $K \geq 0$ is the z component of the total angular momentum quantum number J (helicity), $\sigma = \pm$ and $p = \pm$ are the electronic and total parity, respectively.

Reaction probabilities $P^{Jp}_{e_0 v_0 j_0 K_0}(E_{\rm col})$ at J, p, and collision energy $E_{\rm col}$ depend on the initial rovibronic state, labeled by the electronic e_0, vibrational v_0, rotational j_0, and helicity K_0 quantum numbers. These probabilities are obtained through the real wavepacket (WP) formalism of Gray and Balint-Kurti [8, 9] with a scaled and shifted Hamiltonian $\hat{H}_s$. We recursively solve an *arccos* mapping of the equation of motion, with an initial WP $|\psi_0\rangle = |a_0\rangle + i|b_0\rangle$ and

$$|a_1\rangle = \hat{H}_s|a_0\rangle - (1 - \hat{H}_s^2)^{1/2}|b_0\rangle, \quad \text{first complex propagation,} \tag{1}$$

$$|a_{n+2}\rangle = 2\hat{H}_s|a_{n+1}\rangle - |a_n\rangle, \quad \text{other real Chebyshev propagations.} \tag{2}$$

At the end of the propagation, the quenching (q) or proton exchange-quenching (eq) probabilities are calculated through an asymptotic [8] or flux [9] analysis on the final surface. For $OH + H^+$, OH+H, and rovibronic basis states and $J \leq 40$, 45, and 140, respectively.

3. *$OH(X^2\Pi) + H^+$*

For this collision we have considered two elementary quenching channels [3] due to RT interactions,

$$OH(X^2\Pi) + H'^+(^2S) \rightarrow OH^+(X^3\Sigma^-) + H'(^2S) \quad \text{quenching (q),} \tag{3}$$

$$\rightarrow OH'^+(X^3\Sigma^-) + H(^2S) \quad \text{exchange-quenching (eq),} \tag{4}$$

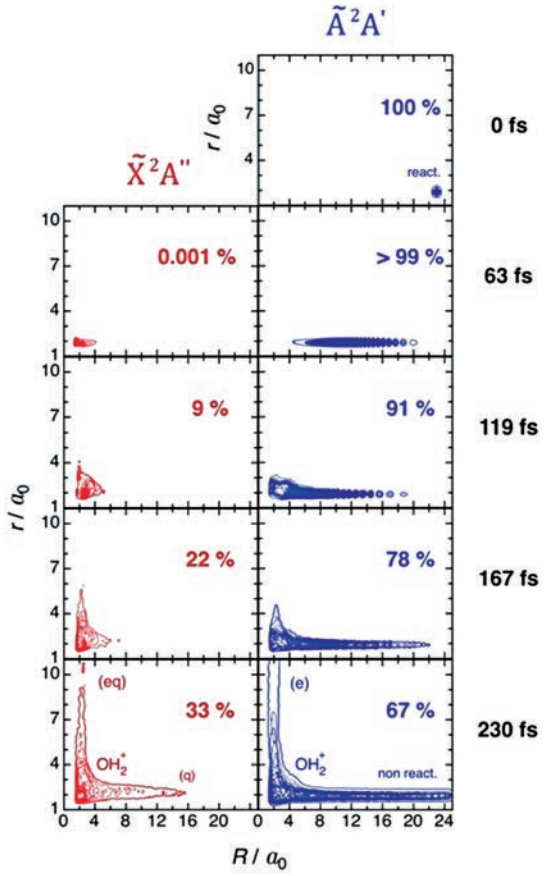

Fig. 1. OH(X²Π)+H'⁺. WP RT norms and γ-averaged densities at 5 times/fs. J=10, p=+, and K_0=0. (e) labels the proton exchange.

which are in competition with the pure proton exchange, a Born-Oppenheimer elementary process that is observable only in isotopic collisions. Reactants and products correlate to the $\tilde{X}^2A''$ and $\tilde{A}^2A'$ adiabatic PESs of OH_2^+, which are strongly bound and are the degenerate components of a linear $^2\Pi$ species. In the R-embedding and considering only the most important $\hat{L}_R$ component, the $^2A''(1)$-$^2A'(2)$ couplings on the angular, adiabatic-electronic, and rotational basis are equal to

$$\begin{aligned} RT_{12} &= \langle j'K'|\langle iA''|\langle K'-p|\hat{H}|K+p\rangle|A'\rangle|jK\rangle \\ &= i\delta_{K'K}\,2K\langle j'K|\left(\frac{B+b}{\sin^2\gamma}-B\right)\langle A''|\hat{L}_R|A'\rangle|jK\rangle \qquad (5) \\ &+iB[\delta_{K',K+1}(1+\delta_{K0})^{1/2}\lambda^+_{JK}+\delta_{K',K-1}(1+\delta_{K1})^{1/2}\lambda^-_{JK}] \\ &\langle j'K'|\cot\gamma\langle A''|\hat{L}_R|A'\rangle|jK\rangle, \end{aligned}$$

and diverge at the linearity. Here $B = (2\mu_R R^2)^{-1}$ and $b = (2\mu_r r^2)^{-1}$, μ_R and μ_r are reduced masses, and $\lambda^{\pm}_{JK} = [J(J+1) - K(K\pm1)]^{1/2}$. Moreover the PESs are modified by σ- and K-diagonal matrix elements of $\hat{L}_R^2$ [3] that diverge at the linearity. We consider all Coriolis couplings in the Born-Oppenheimer matrix elements and in the last row of eq. (5). Here j_0=1 because the reactant OH diatom is in a $^2\Pi$ state.

For investigating the real-time reaction mechanism, we plot in Fig.1 norms and snapshots at five times of the γ-averaged density of a RT WP starting on the $\tilde{A}^2A'$ PES of OH_2^+, at J=10, p = +, and K_0=0. Reactants, intermediate complexes, products (q) and (eq), proton exchange (e), and nonreactive channels are also shown. The WP moves from the initial position at large R towards the interaction region where begins to jump down the ground $\tilde{X}^2A''$ PES after ~63 fs, when the quenching channels open owing to the RT couplings. Metastable OH_2^+ states in the minimum regions of both PESs are then formed at ~119 fs, and the final products appear at ~167 fs. Finally, all product and non-reactive channels are populated at ~230 fs and later on.

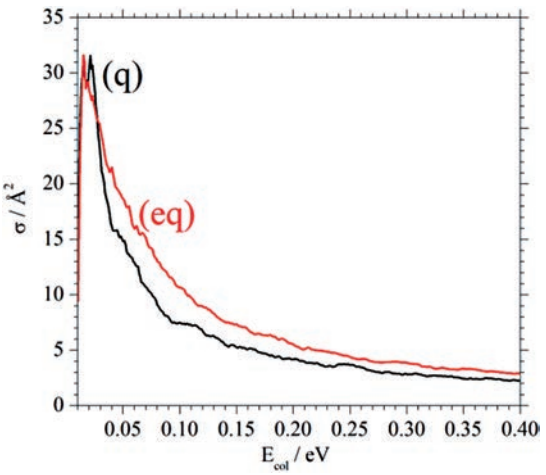

Fig. 2. OH(X²Π)+H'⁺. RT cross sections.

Renner-Teller σ cross sections are presented in Fig. 2 for the quenching (3) and exchange-quenching (4) elementary processes, which are much more reactive than the Born-Oppenheimer proton exchange [3]. In fact the maximum value of σ(q)+σ(eq) is equal to 63.2 Å² at E_{col}=0.15 eV, ~47 times larger than the corresponding value of the proton-exchange reaction. According to the collision energetics, both quenching σ are nearly thresholdless, decrease approximately as $E_{col}^{-1/2}$ above 0.15 eV, and present some small resonances associated with the deep minima of both PESs.

4. *OH($A^2\Sigma^+$)+H(^2S)*

Also OH($A^2\Sigma^+$)+H(^2S) [4] collisions give two quenching products,

$$\begin{aligned} &OH(A^2\Sigma^+)+H'(^2S)\rightarrow OH(X^2\Pi)+H'(^2S) \\ &\qquad\qquad \text{quenching} \qquad (q), \qquad (6) \\ &\qquad\qquad \rightarrow OH'(X^2\Pi)+H(^2S) \\ &\qquad\qquad \text{exchange-quenching} \qquad (eq), \qquad (7) \end{aligned}$$

in competition with proton-exchange and O(^{1}D)+H_2 ($X^1\Sigma_g^+$) products. Reactants and products correlate to the H_2O adiabats $\tilde{X}^1$A' and $\tilde{B}^1$A' that are strongly bound and unbound, respectively, but we use a $\Sigma^+(1)$-$\Pi'(2)$ diabatic representation owing to a conical intersection with couplings

$$CI_{12}=\langle j'K'|\langle\Sigma^+(1)|\langle K'+p|\hat{H}|K+p\rangle|\Pi'(2)\rangle|jK\rangle = \delta_{K'K}\langle j'K|\langle\Sigma^+(1)|\hat{H}^{el}|\Pi'(2)\rangle|jK\rangle. \qquad (8)$$

Considering all Coriolis couplings in the Born-Oppenheimer matrix elements, we contrast in Figs. 3 and 4 nonadiabatic cross sections of both quenching channels these are the most populated channels [4] with $max[\sigma_0(q)+\sigma_0(eq)]=91.5$ Å^2 at 0.004 eV, but now the quenching process (q) is preferred, mainly at $j_0=0$. We also see that the OH rotational excitation inhibits the reactivity and that $\sigma_0(q)$ presents a couple of sharp resonances associated with the large exothermicity of this channel.

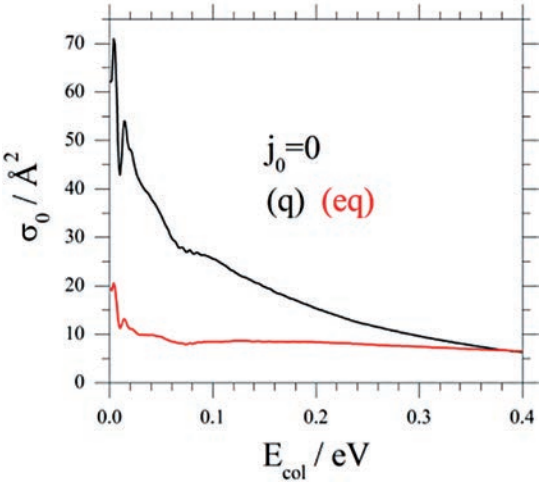

Fig. 3. OH($A^2\Sigma^+$)+H(^2S). $j_0=0$ CI cross sections.

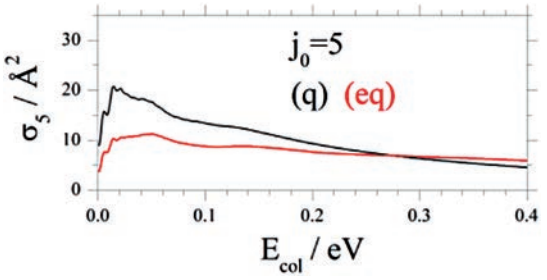

Fig. 4. OH($A^2\Sigma^+$)+H(^2S). $j_0=5$ CI cross sections.

5. *OH($A^2\Sigma^+$)+Kr(^1S)*

Reactants and products of OH($A^2\Sigma^+$)+Kr(^1S)→OH($X^2\Pi$)+Kr(^1S) correlate [6] to three interacting adiabats 1^2A', 2^2A', and 1^2A'' of OHKr, or, equivalently, to the diabats $\Sigma^+(1)$, $\Pi'(2)$, and $\Pi''(3)$. 2A'(Σ^+) is slightly bound and the other states dissociate to OH($^2\Pi$)+Kr, Σ^+ and Π' intersect conically at linearity, and all interact via Renner-Teller effects. On the overall, they are coupled by nine matrix elements with *R*-embedding matrix elements [5]

$$\begin{aligned} &CI_{12}+RT_{12}=\langle j'K|\langle\Sigma^+(1)|\hat{H}^{el}+c_{LL}\hat{L}^2+ \\ &c_{RR}\hat{L}_R^2+c_{xR}\hat{L}_x\hat{L}_R+c_y^{JK}\hat{L}_y|\Pi'(2)\rangle|jK\rangle \\ &RT_{13}=\langle j'K|\langle\Sigma^+(1)|c_R^{JK}\hat{L}_R+c_x^{JK}\hat{L}_x|\Pi''(3)\rangle|jK\rangle, \qquad (9) \\ &RT_{23}=\langle j'K|\langle\Pi'(2)|c_R^{JK}\hat{L}_R+c_x^{JK}\hat{L}_x|\Pi''(3)\rangle|jK\rangle \end{aligned}$$

non considering Coriolis couplings that are highly computer-time demanding. All *c* coefficients depend on the Jacobi coordinates and three of them on *J* and *K* also. The $\hat{L}_R$ coupling in R_{23} was previously considered in other works [3 and Refs. therein] but other seven $\hat{L}$ couplings are fully new and c_{RR}, c_{xR}, c_R^{JK} and c_x^{JK} diverge at linearity.

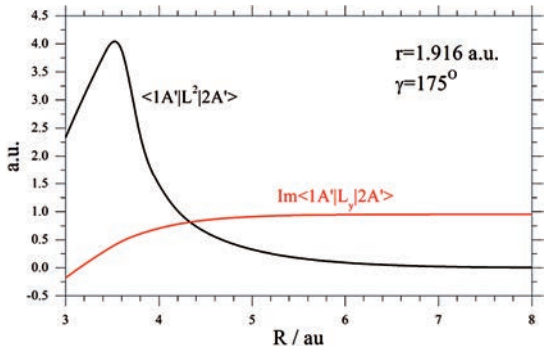

Fig. 5. OH($A^2\Sigma^+$)+Kr(^1S). $r=1.916$ a.u. and $\gamma=175°$.
$\hat{L}^2$ and $\hat{L}_y$ couplings in *r*-embedding and adiabatic representation.

The couplings in eq. (9) are calculated from those MOLPRO [10] in the *r*-embedding and adiabatic representation, and two of the latter are plotted in Fig. 5 at r=1.916 a.u. and γ=175°.

We see that $\langle 1A'|\hat{L}^2|2A'\rangle$ can be very large, up to ~4 a.u., and Im $\langle 1A'|\hat{L}_y|2A'\rangle$ too arrives at 1 a.u. at long range. Nevertheless, these RT couplings near vanish when multiplied by their coefficients c_{LL} and c_y^{JK} in the first row of eq. (9), so that the Σ^+-Π' interaction is essentially due to the conical intersection.

Finally, Fig. 6 shows four quenching probabilities at J=50, j_0=K_0=0 (black) and 1 (red), resolved on the final diabats Π' and Π''. They present many sharp resonances probably associated with rotational states of the $OH(^2\Pi)$ products and to the large exothermic character of the quenching. The $OH(^2\Sigma^+)$ ground rotational state is more or less reactive than the first excited one for the Π' or Π'' elementary channel, respectively, and the former species is favored on the overall. Other probabilities and preliminary cross sections confirm these results.

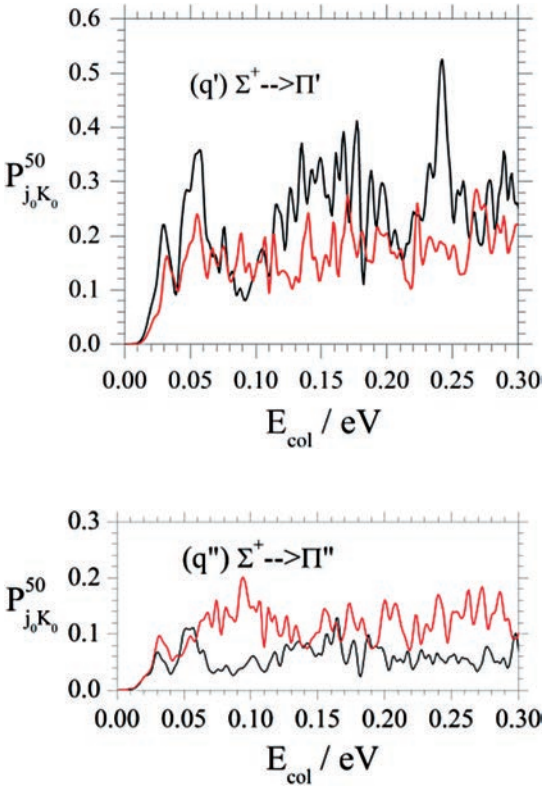

Fig. 6. $OH(A^2\Sigma^+)$+$Kr(^1S)$. Nonadiabatic quenching probabilities at J=50, j_0=K_0=0(black), and 1(red). Above: $\Sigma^+\rightarrow\Pi'$. Below: $\Sigma^+\rightarrow\Pi''$.

6. *Conclusions*

Nonadiabatic interactions between electronic states are not usually considered in astrochemistry and even the largest tables of rate constants [11] or very recent results [12] rely on the Born-Oppenheimer approximation of noninteracting states. Nevertheless, this is not correct in many cases as we have here shown for OH and OH* electronic quenchings and in [2] for He^++H_2 dissociative charge transfer.

We review here some works where we performed large-scale electronic calculations, used *ab initio* nonadiabatic Hamiltonians, solved the time-dependent Schrödinger equation, and transformed from time- to energy-domain for obtain the nonadiabatic quantum dynamics of three quenching collisions. The comparison between nonadiabatic couplings points out their relative importance, the analysis of the wavepacket shows visually the time-dependent mechanism, and the collision dynamics is quantitatively investigated by calculating quenching probabilities and cross sections. In closing, we just report two theoretical findings: the rate constant for quenching plus exchange-quenching in OH+H^+ or in OH*+H from 300 to 400 K represents the 96% or 83% of the total rate, respectively.

Acknowledgments

We are very grateful to A. Bernini, P. Defazio, M. González, and to the Dipartimento di Biotecnologie, Chimica, e Farmacia, Università di Siena, Italy, for invaluable computer resources.

REFERENCES

[1] R. Güsten, H. Wiesemeyer, D. Neufeld, *et al.* Astrophysical detection of the helium hydride ion HeH^+, Nature 568 (2019) 357.

[2] D. De Fazio, A. Aguado, C. Petrongolo, Non-adiabatic quantum dynamics of the dissociative charge transfer He^++H_2→He+H+H^+, Front. Chem. 7 (2019) 249.

[3] P. Gamallo, S. Akpinar, P. Defazio, C. Petrongolo, Nonadiabatic Renner-Teller quantum dynamics of $OH(X^2\Pi)$+H^+ reactive collisions, Phys. Chem. Chem. Phys. 19 (2017) 4454.

[4] P. Gamallo, S. Akpinar, P. Defazio, C. Petrongolo, Conical-intersection quantum dynamics of $OH(A^2\Sigma^+)$+$H(^2S)$ collisions, J. Chem. Phys. 139 (2013) 094303.

[5] P. Gamallo, A. Zanchet, F. J. Aoiz, C. Petrongolo, unpublished.

[6] T. Perkins, D. Herráez-Aguilar, G. McCrudden, J. Klos, F. J. Aoiz, M. Brouard, Surface-hopping trajectories for $OH(A^2\Sigma^+)$+Kr: extension to the 1A'' state, J. Chem. Phys. 142 (2015) 144307.
[7] C. Petrongolo, Nonadiabatic theory of triatomics: general formalism and application to Renner-Teller and conical intersection effects, J. Chem. Phys. 89 (1988) 1297.
[8] S. K. Gray, G. G. Balint-Kurti, Quantum dynamics with real wave packets, including application to three dimensional (J=0) D+H_2→HD+D reactive scattering, J. Chem. Phys. 108 (1998) 950.
[9] A. J. H. M. Meijer, E. M. Goldfield, S. K. Gray, G. G. Balint-Kurti, Flux analysis for calculating reaction probabilities with real wave packets, Chem. Phys. Lett. 293 (1998) 270.
[10] H.-J. Werner, P. J. Knowles, G. Knizia, F. T. Manby, M. Schülz, *et al*., MOLPRO version 2012.1, a package of *ab initio* programs, 2012, http://www.molpro.net.
[11] P. C. Stancil, S. Lepp, A. Dalgarno, The deuterium chemistry in the early Universe, ApJ. 509 (1998) 1.
[12] Proceedings of Astrochem2@2018, II Italian Workshop on Astrochemistry, June 13-16, 2018, Follonica, Italy.